Appendix A. Supplementary data

Facile surface improvement of $LaCoO_3$ perovskite with high activity and water resistance towards toluene oxidation: Ca substitution and citric acid etching

Hanlin Chen [a, c, d], Gaoling Wei [b], Xiaoliang Liang [a, c, d] *, Peng Liu [e] *, Yunfei Xi [f], Jianxi Zhu [a, c, d]

[a] CAS Key Laboratory of Mineralogy and Metallogeny, Guangdong Provincial Key Laboratory of Mineral Physics and Materials, Guangzhou Institute of Geochemistry, Chinese Academy of Sciences, Guangzhou 510640, P.R. China;

[b] Guangdong Key Laboratory of Integrated Agro-Environmental Pollution Control and Management, Guangdong Institute of Eco-Environmental Science & Technology, Guangzhou 510650, P.R. China;

[c] Institutions of Earth Science, University of Chinese Academy of Sciences, Beijing 100049, P.R. China;

[d] University of Chinese Academy of Sciences, Beijing 100049, P.R. China.

[e] School of Environment and Energy, South China University of Technology, Guangzhou 510006, China;

[f] School of Earth and Atmospheric Sciences, Queensland University of Technology (QUT), 2 George Street, Brisbane, QLD 4001, Australia.

~~Text S1. Procedures for char~~acterization

*Corresponding author. Tel: +86 20 85290075, Fax: +86 20 85290075, E-mail: liangxl@gig.ac.cn (X.L. Liang) & liupeng@scut.edu.cn (P. Liu).

*Corresponding author. Tel: +86 20 85290075, Fax: +86 20 85290075, E-mail: liangxl@gig.ac.cn (X.L. Liang) & liupeng@scut.edu.cn (P. Liu).

The element composition in catalyst or etching supernatant was obtained by inductively coupled plasma atomic emission spectroscopy (ICP-AES).

Powder X-ray diffraction patterns (PXRD) were recorded on a Bruker D8 advance diffractometer with Cu Kα radiation.

The N_2 adsorption-desorption isotherm was conducted on a Micromeritics ASAP 2020 apparatus at 77 K. More than 1 g sample was used in each test to ensure the accuracy of BET specific surface area and pore volume. Before analysis, the sample was degassed under vacuum at 150 ^{o}C for 12 h to remove adsorbed species. The BET specific surface area was calculated by multi-point BET method and the pore volume was obtained from the N_2 relative pressure at 0.99.

X-ray photoelectron spectroscopy (XPS) was analyzed with a Thermo Scientific K-Alpha instrument equipped with an Al Kα radiation.

Electron spin resonance (ESR) measurements were operated at a Bruker A300 spectrometer. Typically, a 5.0 mg portion of sample powder was placed in a quartz-glass sample tube. The settings for the ESR spectrometer were as follows: center field at 3400 G, microwave frequency at 9.85 GHz, power at 19.8 mW, sweep width at 2000 G, and mod amplitude at 1G.

Transmission electron microscopy (TEM) images were acquired using FEI Talos F200S instrument.

For all temperature programmed characterization, the flow rate was set at 30 mL min^{-1}.

The H_2-TPR, O_2-TPD and CO_2-TPD were carried out on Beijing Builder PCA-1200 chemisorption instrument which equipped with a TCD detector, while the H_2O-TPD

was recorded on fixed bed apparatus with a mass spectrometry detector.

The hydrogen temperature programmed reduction (H_2-TPR) was evaluated in the range of 30-800 °C at a heating rate of 10 °C min^{-1}. The 50.0 mg sample was preheated at 250 °C under Ar for 30 min. The H_2 consumption was estimated by curve-fitting method using standard CuO sample as calibration.

The temperature programmed desorption of oxygen (O_2-TPD) was evaluated in the range of 40-550 °C at a heating rate of 10 °C min^{-1} under He flow. The 100.0 mg sample was pretreated at 250 ^oC for 1 h and cooled to 40 ^oC under O_2.

For the temperature programmed desorption of CO_2 (CO_2-TPD), 100.0 mg of the sample was first preheated at 400 °C in 20 % O_2/He for 1 h, cooled to 30 °C, and swept by He for another 1 h. Pure CO_2 was introduced into the catalyst bed for 30 min. The He flow was then purged through sample for 1 h to remove physisorbed CO_2. After that, the sample was heated from 30 to 250 °C at a ramp of 10 °C min^{-1} under He flow.

Prior to the temperature programmed desorption of water (H_2O-TPD), the 100.0 mg sample was first pretreated with He at 120 °C, and then purged with H_2O/He until the saturation adsorption of H_2O. After swept by pure He for 1 h at room temperature, the sample was heated to 500 °C to record the mass signal of H_2O.

Text S2. Calculation of the apparent activation energy

The discrepancy in the catalytic activity of the as-prepared catalysts was further manifested by the apparent activation energy (Ea, kJ mol^{-1}), which was evaluated by Arrhenius plots (Eq. (1)):

$$r = A \exp(-Ea/RT)\ [O_2]^a\ [\text{toluene}]^b \quad (1)$$

where r is reaction rate of toluene (μmol g^{-1} s^{-1}); A is pre-exponential factor, R is molar gas constant, 8.314 J mol^{-1} K^{-1}; and a and b were the reaction orders for O_2 and toluene, respectively.

According to previous studies, [1] the oxidation of VOCs over metal oxides in the presence of excess oxygen follows first-order and zero-order kinetics with respect to the concentrations (C, μmol g^{-1}) of toluene and oxygen, respectively. Thus, in this study, the catalytic oxidation of toluene by excess oxygen obeys first-order kinetics towards the toluene concentration (C, umol g^{-1}), (Eq. (2)):

$$r = kC = A \exp(-Ea/RT)\ C \quad (2)$$

where k is the rate constant (s^{-1}), calculated by the reaction rates and toluene conversion.

Then, taking the natural log of both sides, Eq. (2) can be transformed to Eq.(3):

$$lnr = -\ Ea/RT + lnA\ C \quad (3)$$

The activation energy (E_a) was calculated from the fitted least squares of Eq.(3).

Text S3. Calculation of the specific reaction rate constant

The specific reaction rate constant (R_s) of $LaCoO_3$-based catalysts was defined as the number of toluene molecules converted over catalysts per second per unit area (Eq. (4)).

$$R_s = C_{toluene} \times X_{toluene} \times V_{gas}/S \quad (4)$$

where $C_{toluene}$ is the concentration of toluene in gas mixture (ppm), $X_{toluene}$ is the conversion of toluene (%), V_{gas} is the total flow rate (μmol s^{-1}), and S was the specific surface area (m^2 g^{-1}).

Text S4. Calculations of toluene conversion, CO_2 selectivity, and change in CO_2 selectivity.

The toluene conversion (X) rate was obtained from the following Eq. (5):

$$X = C^*_{toluene} - C_{toluene} / C^*_{toluene} \times 100\% \quad (5)$$

where $C_{toluene}$ and $C^*_{toluene}$ are the concentration of toluene in the outlet and inlet gas flow, respectively. The concentration of toluene was analyzed by a gas chromatograph (Agilent 7820A) equipped with an FID detector.

The CO_2 selectivity was defined in the following Eq. (6) [2]:

$$CO_2 \text{ selectivity} = CO_2 / [7*(C^*_{toluene} - C_{toluene})] \times 100\% \quad (6)$$

The change in CO_2 selectivity (ΔS) was calculated from the following Eq. (7):

$$\Delta S = S^* - S_{H_2O} \quad (7)$$

where S^* and S_{H_2O} are the CO_2 selectivity before and after the introduction of 5 vol% H_2O in feed gas, respectively.

Table S1. Summary of the catalytic activity of reported cobalt-related catalysts towards toluene oxidation.

Catalysts	Surface area/m^2 g^{-1}	Concentration/ppm	GHSV/mL g^{-1} h^{-1}	T50 /°C	T90 /°C	Ref.
Co_3O_4	51.7	1000	20000	195	215	[3]
spherical Co_3O_4	20.9	1000	20000	249	266	[4]
Co_3O_4-C[a]	83.1	1000	48000	240	248	[5]
Co_3O_4-P[b]	58.8	1000	48000	243	254	[5]
Co_3O_4-N[c]	25.9	1000	48000	250	259	[5]
3D-Co_3O_4	84.6	1000	48000	229	238	[6]
2D-Co_3O_4	24.9	1000	48000	242	249	[6]
1D-Co_3O_4	24.9	1000	48000	245	257	[6]
CoMn0.5	249	1200	60000	271	311	[7]
CoCoO	55.5	191	60000	186	205	[8]
Co30Ce	33	1000	36000	233	260	[9]
CoAlO	88.6	2000	60000	307	319	[10]
CoCe-P[d]	89	1000	60000	212	230	[11]
Montmorillonite pillared by Co_3O_4	53	1000	30000	284	297	[12]
Co_3O_4/3DOM-ESFO[e]	24.1	1000	20000	251	269	[13]
Au/Co_3O_4	1.6	146	14690	200	300	[14]
Ru/Co_3O_4-MOF[f]	80	1000	60000	231	238	[15]
Pd/Co3AlO	93	800	30000	220	230	[16]
Ag–CoAlO	69.5	2000	60000	293	300	[10]
Pt–CoAlO	81.1	2000	60000	282	289	[10]

Pd–CoAlO	51.8	2000	60000	222	226	[10]
Ce–Co (CX)[g]	131	266	60000	231	246	[17]
Ce–Co (EM)[h]	109	266	60000	237	253	[17]
La–Co (CX)[i]	92	266	60000	307	350	[17]
La–Co (EM)[j]	68	266	60000	258	283	[17]
LCO-1[k]	5.81	1000	60000	206	223	[18]
Hollow spherical $LaCoO_3$	20.7	1000	20000	220	237	[4]
$La_{0.6}Sr_{0.4}Co_{0.9}Fe_{0.1}O_3$	21	1000	20000	220	239	[19]
$La_{0.6}Sr_{0.4}CoO_{2.76}$	15	1000	20000	212	220	[20]
$La_{0.98}Ag_{0.02}CoO_3$	7.5	1000	60000	225	251	[21]
$LaCoO_3$/SBA-15	353	1000	20000	284	310	[22]
Co_3O_4/3DOM-LSCO[l]	29.7	1000	20000	210	227	[23]
Ag/LCO-450	11.9	1000	60000	239	279	[21]
$La_{0.9}Ca_{0.1}CoO_3$-CA	11.2	1000	60000	195	202	This study

[a]Co_3O_4-C, 3D hierarchical cubes-stacked Co_3O_4 microspheres; [b]Co_3O_4-P, 3D hierarchical plates-stacked Co_3O_4 flower; [c]Co_3O_4-N, 3D hierarchical needles-stacked Co_3O_4 twospheres with an urchin-like structure. [d]CoCe-P, CoO_x/CeO_2 nanoparticles. [e]Co_3O_4/3DOM-ESFO, 3DOM $Co_3O_4/Eu_{0.6}Sr_{0.4}FeO_3$. [f]Ru/$Co_3O_4$-MOF, Ru/ Co_3O_4-MOF were prepared through a metal–organic frameworks (MOFs)-templated method. [g-j]Ce-Co and La-Co mixed oxides are prepared by evaporation method (EM) and exotemplating method (EX). [k]LCO-1, acetic acid treated LCO for 1 h. [l]Co_3O_4/3DOM-LSCO, Co_3O_4/3DOM $La_{0.6}Sr_{0.4}CoO_3$.

Table S2. Summary of the reported data on the catalytic oxidation of gaseous toluene in a humid stream.

Sample	Test conditions	$X(T)$ [a]	Ref.
$CoMnO_x$	1000 ppm toluene, GHSV = 60,000 mL g^{-1} h^{-1}, 5 vol.% H_2O	90% (250 °C)	24
$Mn_{0.3}Zr_{0.7}O_2$	1000 ppm toluene, GHSV = 60,000 mL g^{-1} h^{-1}, 3 vol.% H_2O	90% (233 °C)	25
$3MnO_x$-$1FeO_y$	1000 ppm toluene, GHSV = 240,000 mL g^{-1} h^{-1}, 10 vol.% H_2O	90% (260 °C)	26
MnO_x/Cr_2O_3	1000 ppm toluene, GHSV = 20,000 mL g^{-1} h^{-1}, 10 vol.% H_2O	90% (270 °C)	27
CoO_x/CeO_2	1000 toluene ppm, GHSV = 60,000 mL g^{-1} h^{-1},5 vol.% H_2O	90% (225 °C)	28
Pd-CoAlO	1000 ppm toluene, GHSV = 60,000 mL g^{-1} h^{-1}, 5 vol.% H_2O	90% (240 °C)	10
Pt-AAO[b]	1000 ppm toluene, GHSV = 40,000 mL g^{-1} h^{-1}, 5.0 vol.% H_2O	90% (230 °C)	29
$MnO_2/LaMnO_3$	1000 toluene ppm, GHSV = 40,000 mL g^{-1} h^{-1}, 2 vol.% H_2O	90% (235 °C)	30
$La_{0.9}Ca_{0.1}CoO_3$-CA	1000 ppm toluene, GHSV = 60,000 mL g^{-1} h^{-1}, 5 vol.% H_2O	90% (205 °C)	This study

[a] $X(T)$ represents toluene conversion (X) at a specific reaction temperature (T).

[b] AAO: Anodic aluminum oxide.

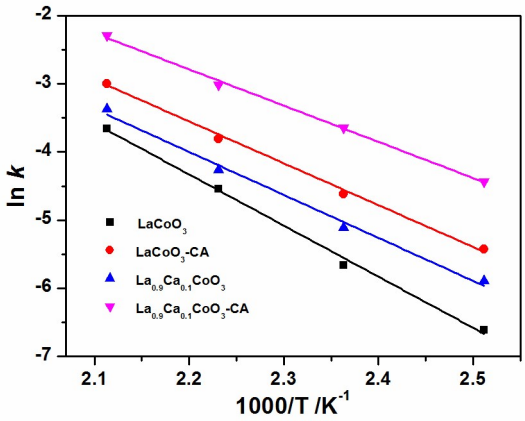

Fig. S1. Arrhenius plots for the oxidation of toluene over $LaCoO_3$-based catalysts. Reaction conditions: [toluene] = 1000 ppm, [O_2] = 20%, catalyst mass = 200.0 mg, total flow rate = 100 mL min^{-1}, and GHSV = 60 000 cm^3 g^{-1} h^{-1}.

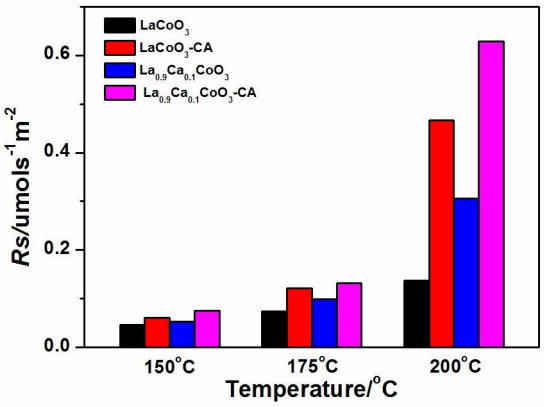

Fig. S2. R_s plots of toluene oxidation over $LaCoO_3$-based catalysts (150, 175, and 200 ^{o}C).

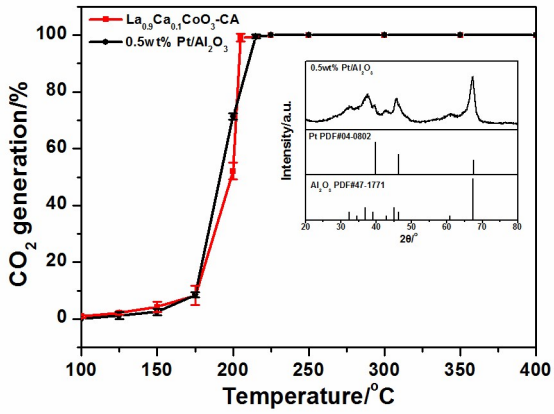

Fig. S3. Comparison of the toluene catalytic activities between $La_{0.9}Ca_{0.1}CoO_3$-CA and 0.5 wt% Pt/Al_2O_3. Reaction conditions: [toluene] = 1000 ppm, [O_2] = 20%, catalyst mass = 100.0 mg, total flow rate = 100 mL min^{-1}, and GHSV = 60 000 cm^3 g^{-1} h^{-1}. The inset shows the XRD pattern of 0.5 wt% Pt/Al_2O_3.

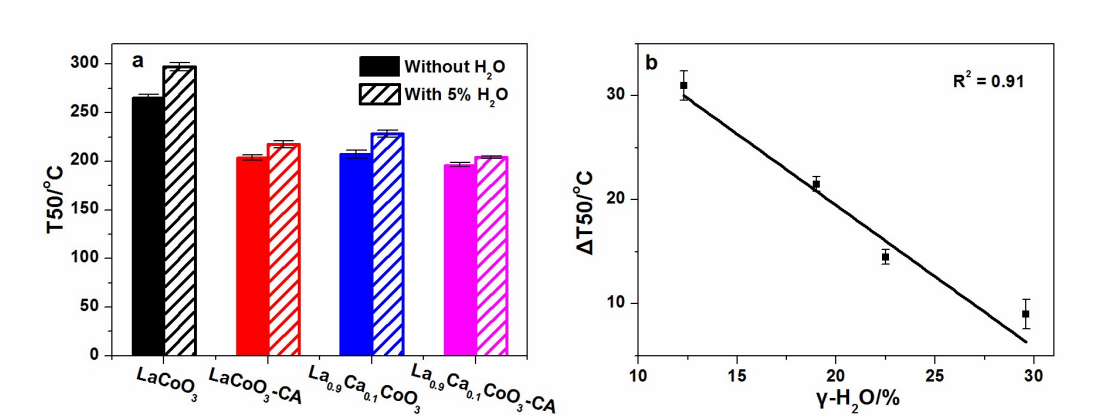

Fig. S4. The T50 of $LaCoO_3$-based samples with/without the presence of 5 vol% H_2O (a) and the relationship between the γ-H_2O and ΔT50 (b).

When 5% H_2O is added into the feed gas, the T50 of all $LaCoO_3$-based catalysts increases. The temperature difference (ΔT50) of $LaCoO_3$ is 32 °C before and after the water addition, while it decreases to 8 °C over $LaCoO_3$-based catalysts subjected to Ca substitution or the citric acid treatment. This illustrates the improvement in the anti-water ability by Ca substitution and the citric acid treatment. Interestingly, the ΔT50 is positively correlated with γ-H_2O, which is generated through the reaction between H_2O and surface active oxygen.

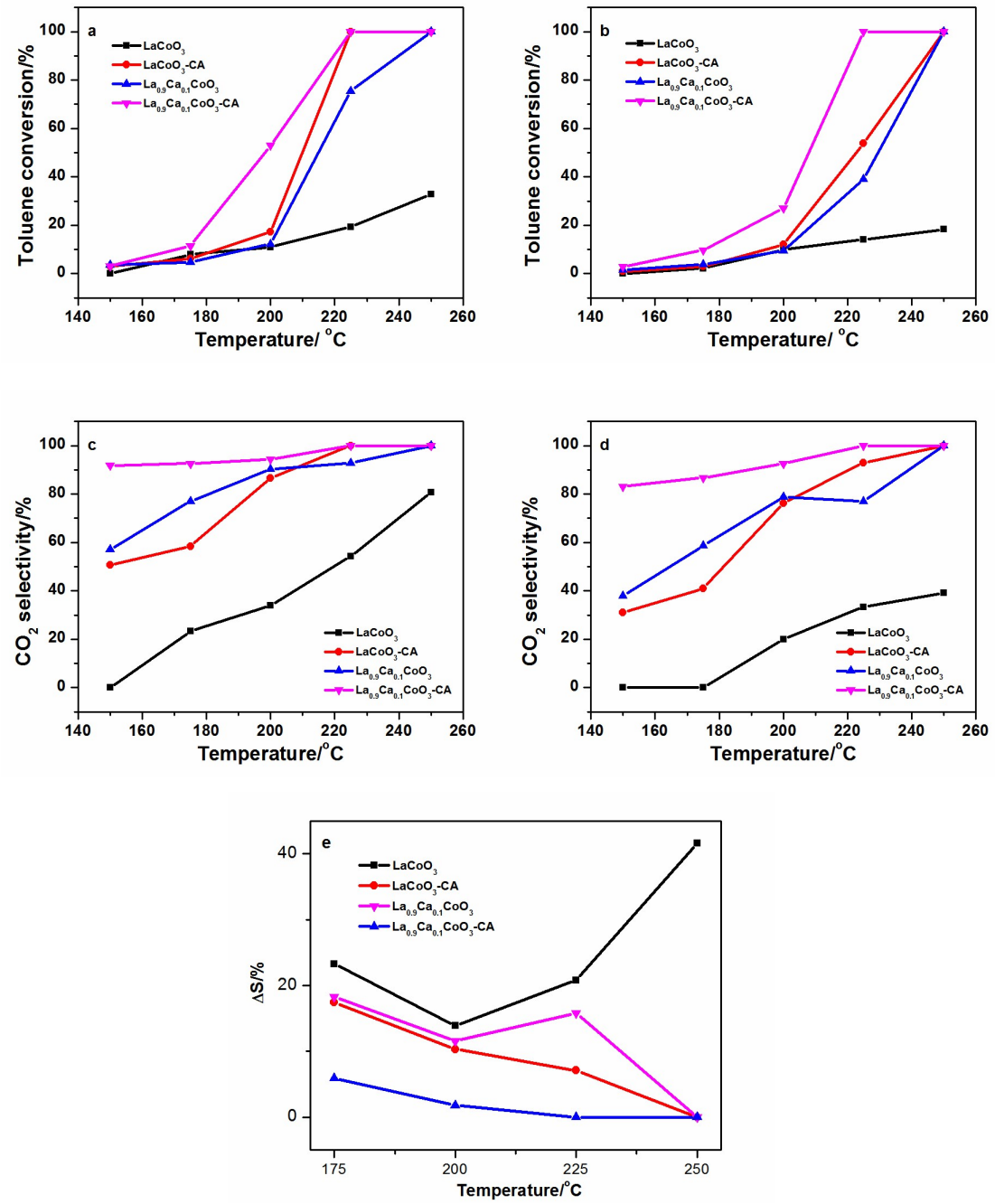

Fig. S5. Toluene conversion and CO_2 selectivity without water (a and c) and with 5 vol% H_2O (b and d) in the feed gas, and the variation of in CO_2 selectivity by H_2O introduction (e).

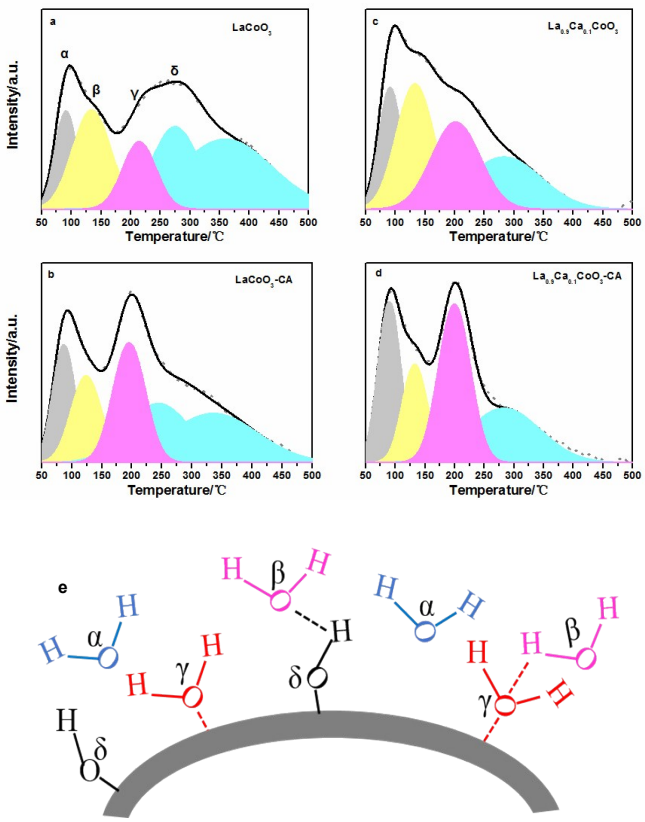

Fig. S6. H_2O-TPD profiles of $LaCoO_3$ (a), $LaCoO_3$-CA (b), $La_{0.9}Ca_{0.1}CoO_3$ (c), and $La_{0.9}Ca_{0.1}CoO_3$-CA (d), and the schematic diagram of four types of surface water (e).

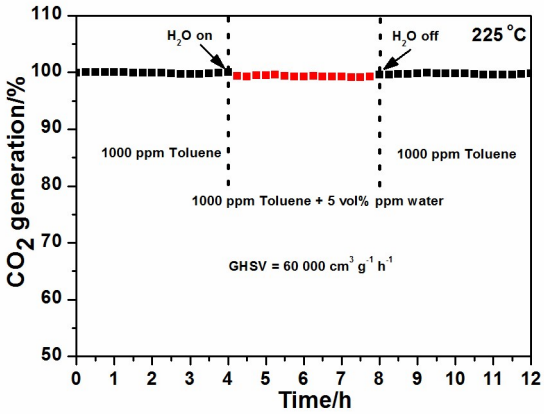

Fig. S7. The anti-water ability and stability of $La_{0.9}Ca_{0.1}CoO_3$-CA at 225 °C in the presence of water vapor. Reaction conditions: [toluene] = 1000 ppm, [O_2] = 20%, [H_2O] = 5vol%, catalyst mass = 100 mg, total flow rate = 100 mL min^{-1}, and GHSV = 60000 cm^3 g^{-1} h^{-1}.

References

1. M. Alifanti, M. Florea, S. Somacescu and V.I. Parvulescu, *Appl. Catal. B-Environ.*, 2005, **60**, 33-39.
2. G. M. Bai, H. X. Dai, J. G. Deng, Y. X. Liu, F. Wang, Z. X. Zhao, W. G. Qiu and C. T. Au, *Appl. Catal. A-Gen.*, 2013, **450**, 42-49.
3. J. Wang, A. Yoshida, P.F. Wang, T. Yu, Z.D. Wang, X.G Hao, A. Abudula and G. Guan, *Appl. Catal. B-Environ.*, 2020, **217**, 118941.
4. Y. X. Liu, H. X. Dai, J. G. Deng, L. Zhang, Z. X. Zhao, X. W. Li, Y. Wang, S. H. Xie, H. G. Yang and G. S. Guo, *Inorg. Chem.*, 2013, **52**, 8665-8676.
5. Q. M. Ren, S. P. Mo, R. S. Peng, Z. T. Feng, M. Y. Zhang, L. M. Chen, M. L. Fu, J. L. Wu and D. Q. Ye, *J. Mater. Chem.*, 2018, **6**, 498-509.
6. Q. M. Ren, Z. T. Feng, S. P. Mo, C. L. Huang, S. J. Li, W. X. Zhang, L. M. Chen, M. L. Fu, J. L. Wu and D. Q. Ye, *Catal. Today*, 2019, **332**, 160-167.
7. D. A. Aguilera, A. Perez, R. Molina and S. Moreno, *Appl. Catal. B-Environ.*, 2011, **104**, 144-150.
8. S. P. Mo, S. D. Li, J. Q. Li, Y. Z. Deng, S. P. Peng, J. Y. Chen and Y. F. Chen, *Nanoscale*, 2016, **8**, 15763-15773.
9. L. F. Liotta, M. Ousmane, G. Di Carlo, G. Pantaleo, G. Deganello, A. Boreave and A. Giroir-Fendler, *Catal. Lett.*, 2009, **127**, 270-276.
10. S. Zhao, K. Z. Li, S. Jiang and J. H. Li, *Appl. Catal. B-Environ.*, 2016, **181**, 236-248.
11. H. J. Wu, L. D. Wang, Z. Y. Shen and J. H. Zhao, *J. Mol. Catal. A-Chem.*, 2011,

351, 188-195.

12. A. Rokicinska, P. Natkanski, B. Dudek, M. Drozdek, L. Litynska-Dobrzynska and P. Kustrowski, *Appl. Catal. B-Environ.*, 2016, **195**, 59-68.

13. K. M. Ji, H. X. Dai, J. G. Deng, X. W. Li, Y. Wang, B. Z. Gao, G. M. Bai and C. T. Au, Appl. *Catal. A-Gen.*, 2012, **447**, 41-48.

14. H. J. Wu, L. D. Wang, Z. Y. Shen and J. H. Zhao, *J. Mol. Catal. A-Chem.*, 2011, 351, 188-195.

15. X. L. Liu, J. Wang, J. L. Zeng, X. Wang and T. Y. Zhu, *RSC Adv.* 2015, **5**, 52066-52071.

16. P. Li, C. He, J. Cheng, C. Y. Ma, B. J. Dou and Z. P. Hao, *Appl. Catal. B-Environ*, 2011, **101**, 570-579.

17. S. A. C. Carabineiro, X. Chen, M. Konsolakis, A. C. Psarras, P. B. Tavares, J. J. M. Orfao, M. F. R. Pereira and J. L. Figueiredo, *Catal. Today*, 2015, **244** 161-171.

18. Q. L. Yang, D. Wang, C. Z. Wang, X. F. Li, K. Z. Li, Y. Peng and J. H. Li, *Catal. Sci. Technol.*, 2018, **8**, 3166-3173.

19. J. G. Deng, H. X. Dai, H. Y. Jiang, L. Zhang, G. Z. Wang, H. He and C. T. Au, *Environ. Sci. Technol.*, 2010, **44**, 2618-2623.

20. J. G. Deng, L. Zhang, H. X. Dai, H. He and C. T. Au, *Ind. Eng. Chem. Res.*, 2008, **47**, 8175-8183.

21. H. Chen, G. Wei, X. Liang, P. Liu, H. He, Y. Xi and J. Zhu, *Appl. Surf. Sci.*, 2019, **489**, 905-912.

22. J. G. Deng, L. Zhang, H. X. Dai and C. T. Au, *Appl. Catal. A-Gen.*, 2009, **352**, 43-49.

23. X. W. Li, H. X. Dai, J. G. Deng, Y. X. Liu, Z. X. Zhao, Y. Wang, H. G. Yang and C. T. Au, Appl, *Catal, A-Gen.*, 2013, **458**, 11-20.

24. W. T. Zhao, Y. Y. Zhang, X. W. Wu, Y. Y. Zhan, X. Y. Wang, C. T. Au and L. L. Jiang, *Catal. Sci. Technol.*, 2018, **8**, 4494-4502.

25. X. Q. Yang, X. L. Yu, M. Z. Jing, W. Y. Song, J. Liu and M. F. Ge, *Acs Appl. Mater. Inter.*, 2019, **11**, 730-739.

26. J. Chen, X. Chen, W. J. Xu, Z. Xu, J. Z. Chen, H. P. Jia and J. Chen, *Chem. Eng. J.*, 2017, **330**, 281-293.

27. X. Chen, S. C. Cai, E. Q. Yu, J. Chen and H. P. Jia, *Appl. Surf. Sci.*, 2019, **475**, 312-324.

28. F. Y. Hu, Y. Peng, J. J. Chen, S. Liu, H. Song and J. H. Li, *Appl. Catal. B-Environ.*, 2019, **240**, 329-336.

29. Q. Zhang, H. J. Luan, T. Li, Y. Q. Wu and Y. H. Ni, *Appl. Surf. Sci.*, 2016, **360**, 1066-1074.

30. B. Li, Q. L. Yang, Y. Peng, J. J. Chen, L. Deng, D. Wang, X. W. Hong and J. H. Li, *Chem. Eng. J.*, 2019, **366**, 92-99.